In-situ Growth of Redox-active Metal-Organic Framework on Electrospun Carbon Nanofiber as a Free-Standing Electrode for Flexible Energy Storage Devices

Zahir Abbas, [a] Nissar Hussain, [a] Surender Kumar [c], Shaikh M. Mobin *, [a, b]

[a] Department of Chemistry, Indian Institute of Technology (IIT) Indore, Simrol, Khandwa Road, Indore 453552, India

[b] Center for Advanced Electronics (CAE), Indian Institute of Technology (IIT) Indore, Simrol, Khandwa Road, Indore 453552, India

[c] CSIR-Advanced Materials and Processes Research Institute (CSIR-AMPRI), Hoshangabad Road, Near Habibganj Naka, Bhopal – 462026, India.

*Corresponding author

Email: xray@iiti.ac.in (Shaikh M. Mobin)

Tel.: +91-731-2438752

Efficiency Evaluation

The specific capacity (C g^{-1}) of the electrode was evaluated using the equation 1:

$$Cs = \frac{I}{m}\Delta t \quad (1)$$

where I/m, Δt represent current density, discharge time respectively.

The specific capacitance of as-synthesized electrode materials was evaluated through the GCD curves by using the following relation

$$Cs = \frac{I \times \Delta t}{m \times \Delta V} \quad (2)$$

where I/m, Δt, and ΔV represent current density, discharge time, and the potential range of the GCD profile, respectively.

Furthermore, the energy density (E) and power density (P) of the asymmetric device (ASC) were calculated by the following relations

$$E = \frac{Cs \times \Delta V^2}{2 \times 3.6} \quad (3)$$

$$P = \frac{E}{\Delta t} \times 3600 \quad (4)$$

where C_s, ΔV, and Δt indicate the specific capacitance, potential window, and discharge time of the GCD profile, respectively

Electrochemical measurement in a three-electrode system

Electrochemical measurement in a three-electrode system was studied according to the procedure in literature.[1] The prepared NiFc-MOF@CNF freestanding electrode was carefully cut into 1cm × 1 cm (a mass loading ~2 mg) that was used as a working electrode, Ag/AgCl as a reference electrode, and platinum wire as the counter electrode. To determine the electrochemical performance, 2M KOH aqueous solution was used as an electrolyte, cyclic voltammetry (CV), galvanostatic charge-discharge (GCD) curve measurements, and electrochemical impedance spectroscopy (EIS) was carried out on Autolab work station. The efficiency evaluation was determined by the following equations summarised above. The electrochemical study of pristine NiFc-MOF is studied by drop casting MOF on Ni foam (NF) as a working electrode and the mass loading is around 2 mg by dispersing in ethanol.

PVA/KOH Gel preparation:

The alkaline PVA/KOH polymer electrolyte was prepared by a solution-casting method. Initially, 1.0 g of PVA was dissolved in 25 ml of water with continuous stirring for about 4 h at 80 ℃. After the complete dissolution of the PVA polymer, 1.0 g of KOH (dissolved in 25 ml water by continuous stirring for 5 h at 95 ℃ was added and the resulting solution was continuously stirred until the formation of a homogeneous viscous solution.

Characterization

All the reagents and solvents were purchased from a commercial source without any further purification. For the Powder X-ray diffraction (PXRD) analysis, Cu Kα (0.154 nm) monochromatic radiation was used with a Rigaku Smart Lab X-ray diffractometer. The morphologies were investigated by a Supra55 Zeiss field emission scanning electron microscope (FESEM) and high-resolution transmission electron microscopy (HR-TEM) was performed using (TEM, JEM F200). Brunauer−Emmett−Teller (BET) surface area and Barrett−Joyner−Halenda (BJH) distribution determinations were conducted on an Autosorb iQ (Quantachrome Instruments, version 1.11). X-ray photoelectron spectroscopic (XPS) analysis (XPS, Nexsa, Thermofisher Scientific) incorporating Al Kα as the source of X-ray.

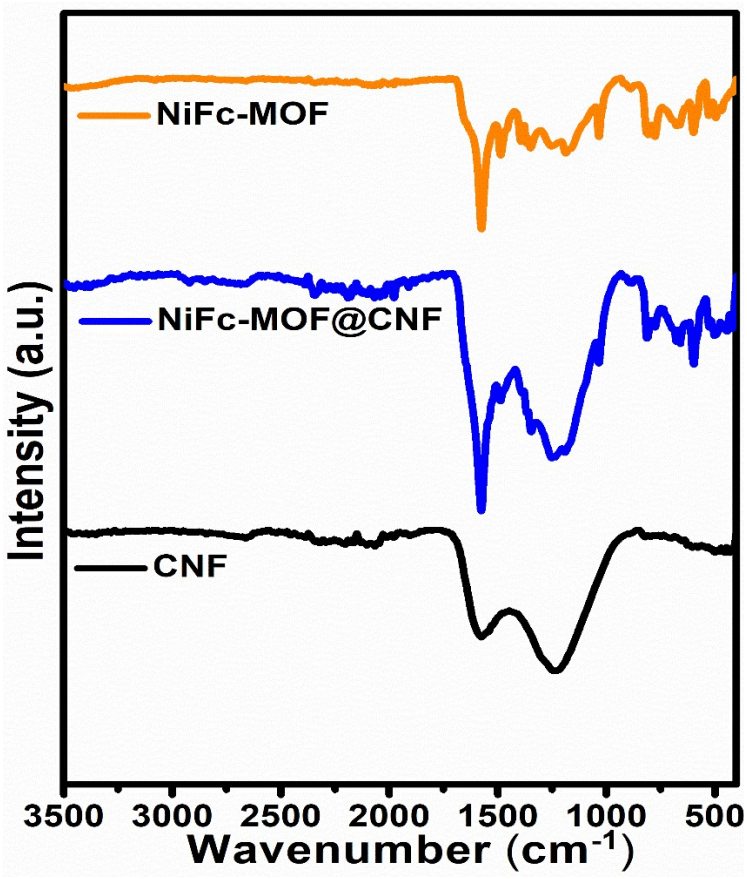

Fig. **S1**. Shows FT-IR analysis of NiFc-MOF@CNF, NiFc-MOF and CNF.

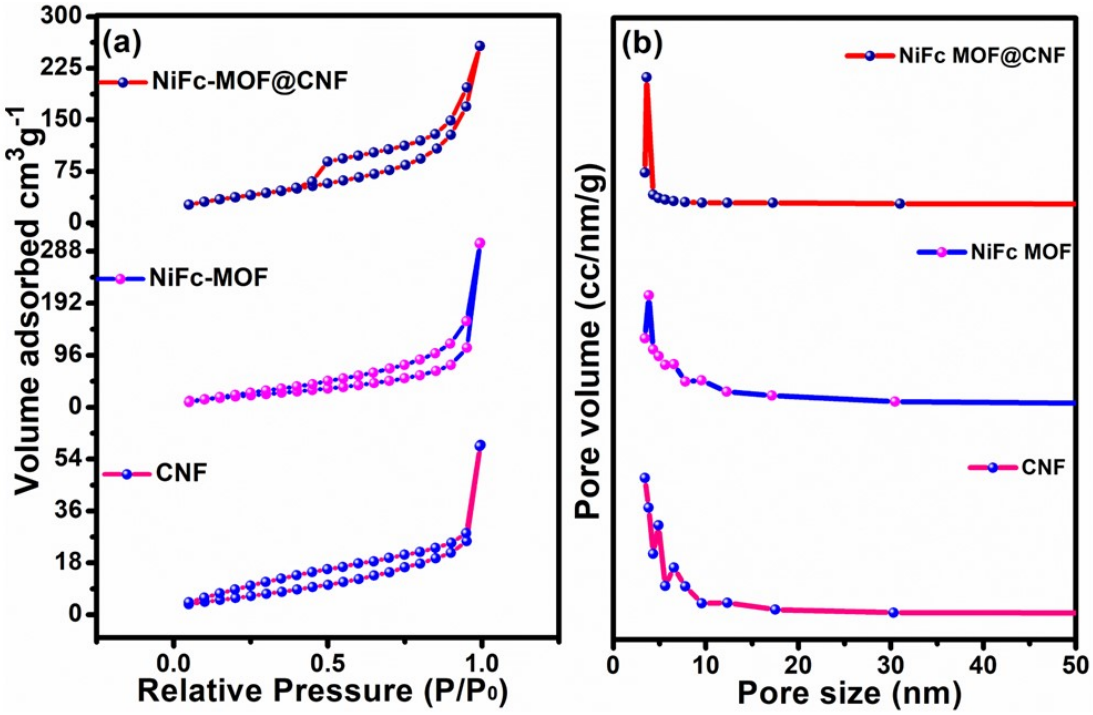

Fig. S2. (a) BET surface area analysis of NiFc-MOF@CNF, NiFc-MOF, and CNF (b) BJH Pore diameter of NiFc-MOF@CNF, NiFc-MOF and CNF.

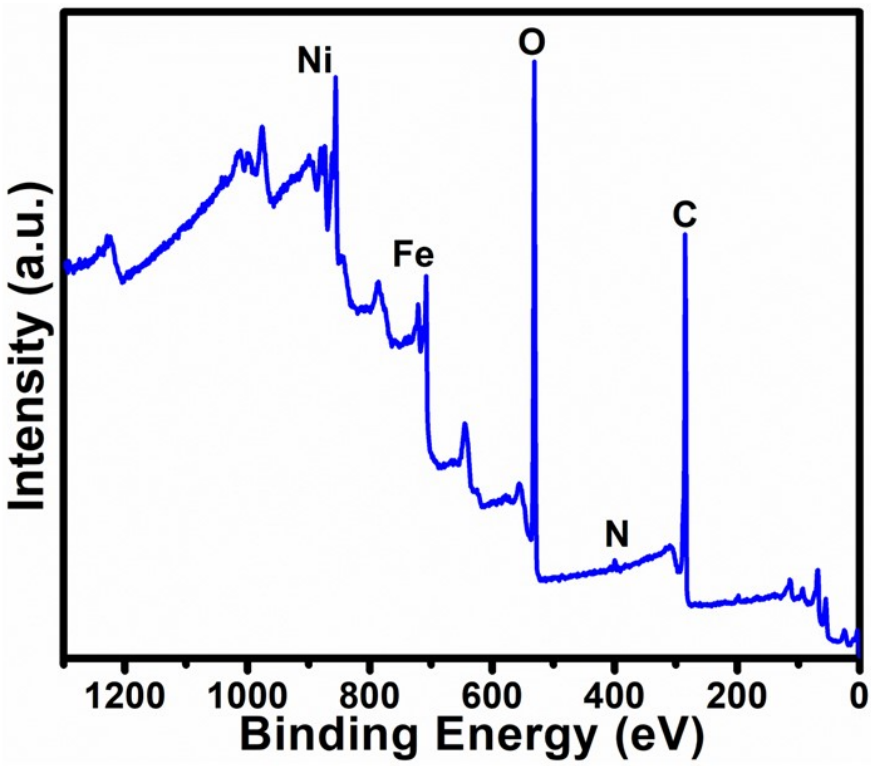

Fig. S3. XPS Survey scan of NiFc-MOF@CNF.

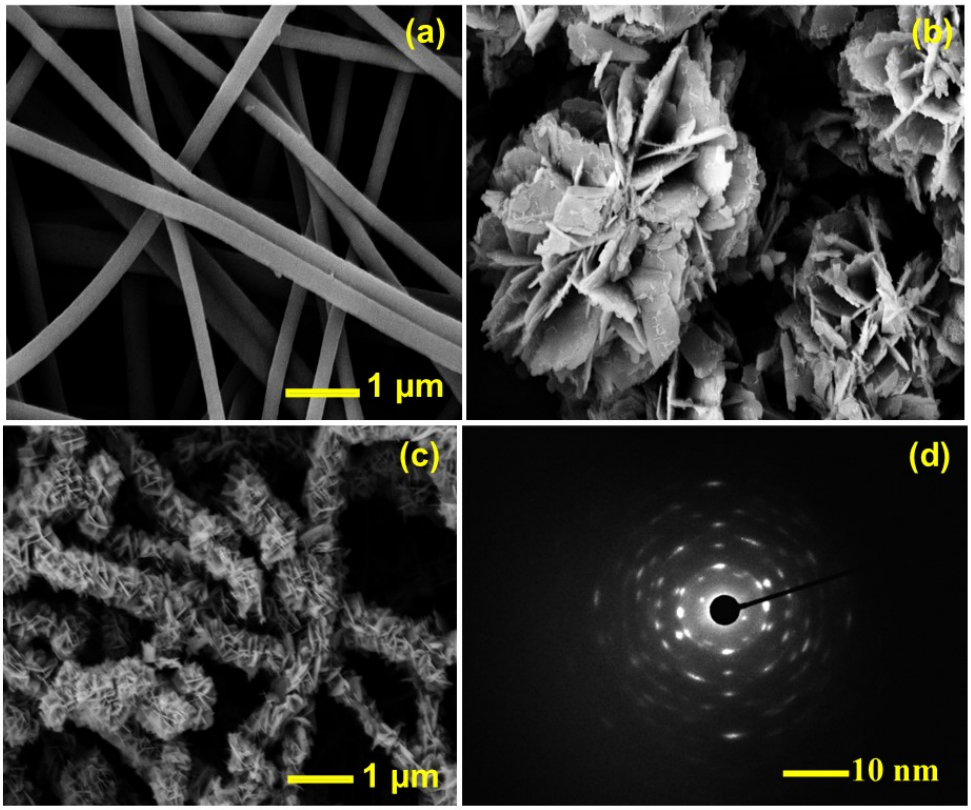

Fig. S4. SEM analysis of (a) CNF (b) NiFc-MOF and (c) NiFc-MOF@CNF at the same magnification range (d) SAED pattern of NiFc-MOF@CNF.

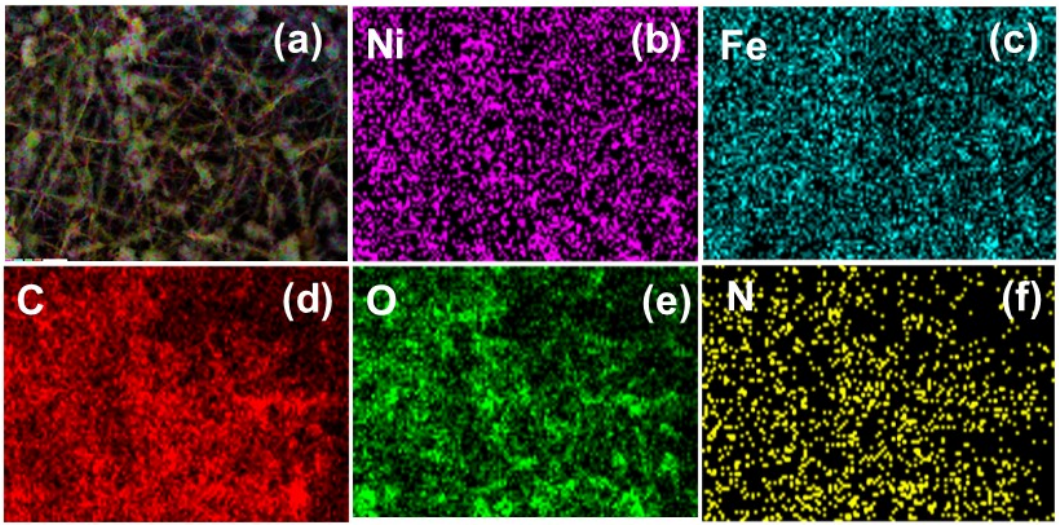

Fig. S5. (a) SEM images and (b-f) EDS analysis shows Ni, Fe, C, N, O present in NiFc-MOF@CNF.

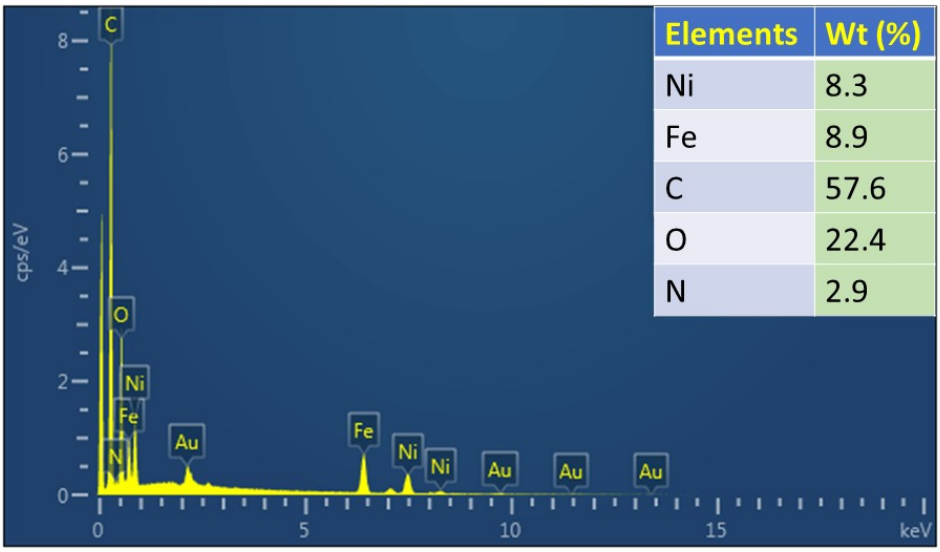

Elements	Wt (%)
Ni	8.3
Fe	8.9
C	57.6
O	22.4
N	2.9

Fig. S6. EDX of NiFc-MOF@CNF with percentage content.

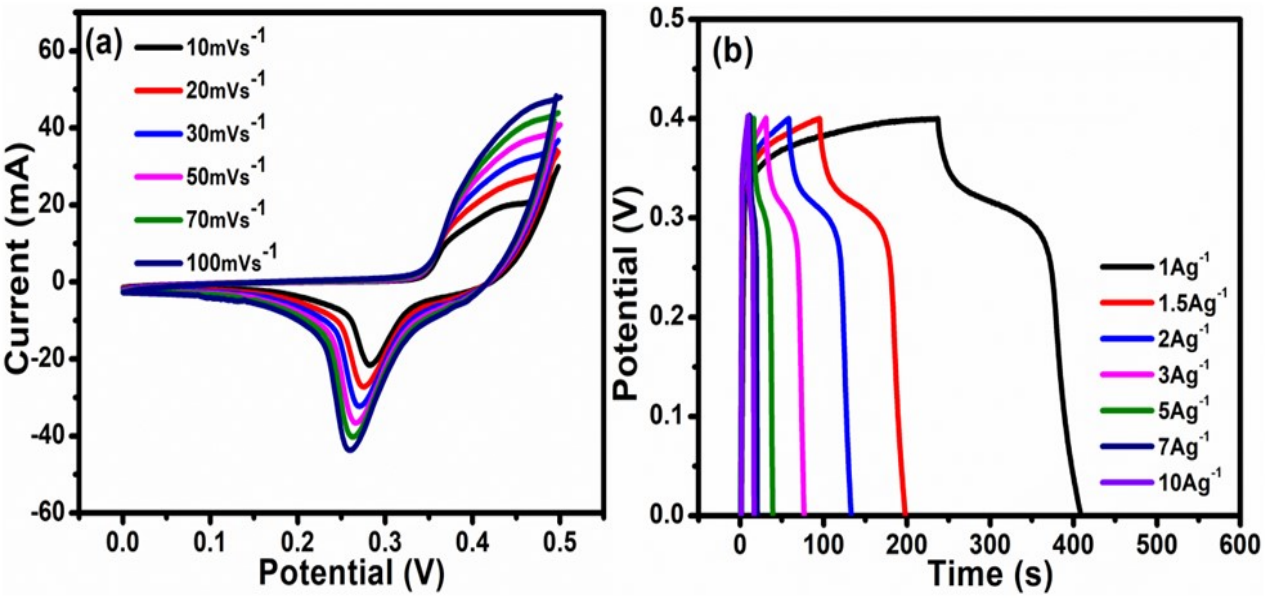

Fig. S7. (a) Cyclic volumetry curve of NiFc-MOF (b) GCD curve of NiFc-MOF.

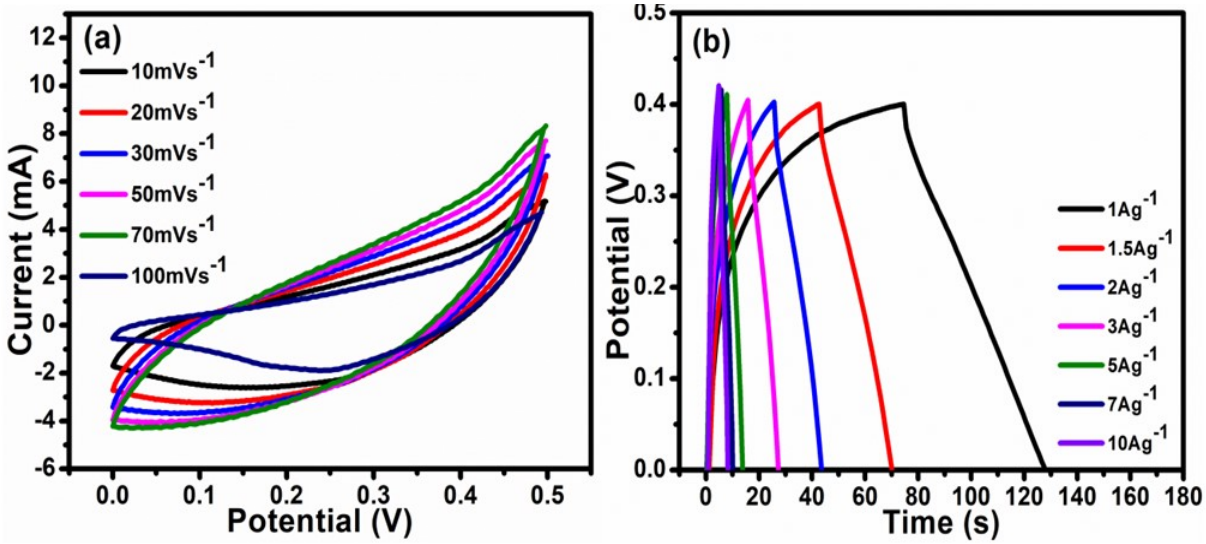

Fig. S8. (a) Cyclic voltammetry curve of CNF (b) GCD curve of CNF.

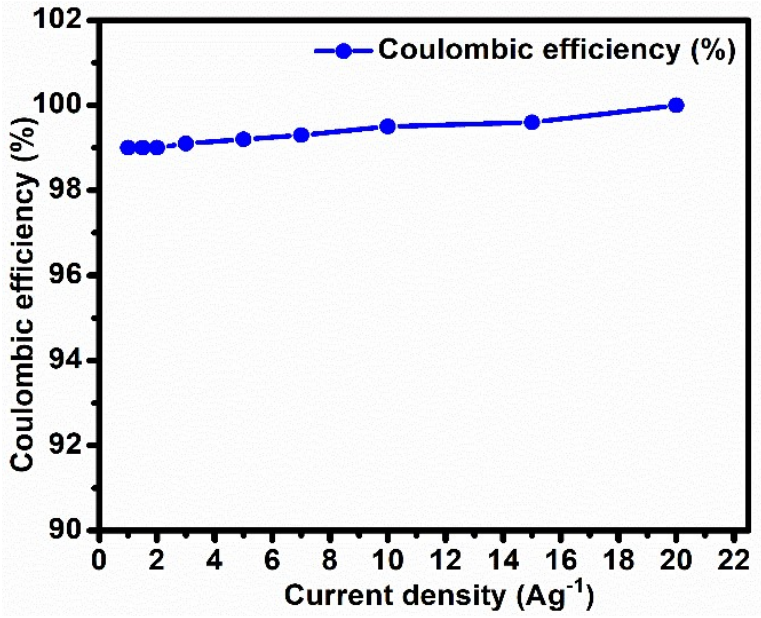

Fig.S9 Shows the coulombic efficiency of NiFc-MOF@CNF electrode material.

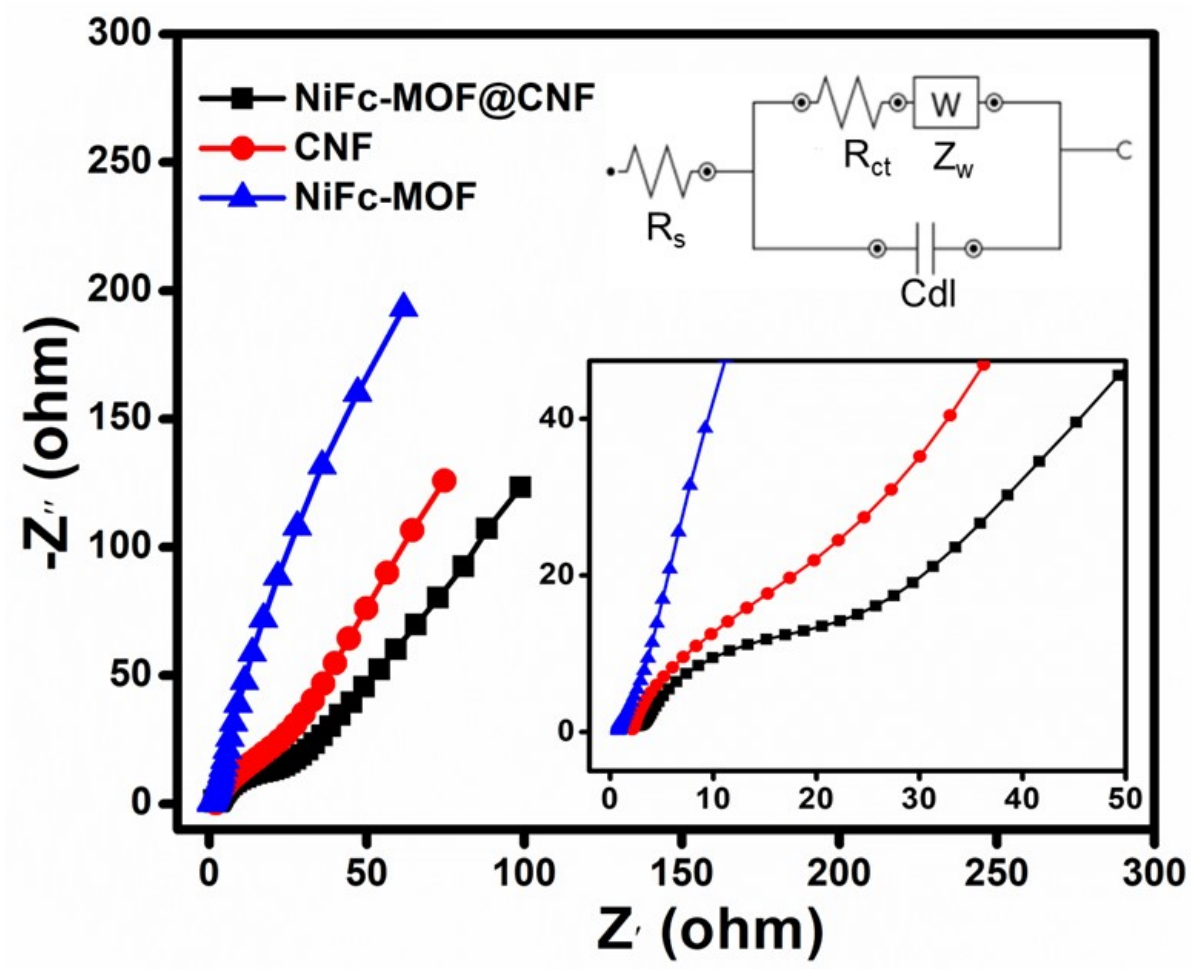

Fig. S10. EIS Nyquist plot of Nifc-MOF@CNF, Nifc-MOF, and CNF for the three-electrode system.

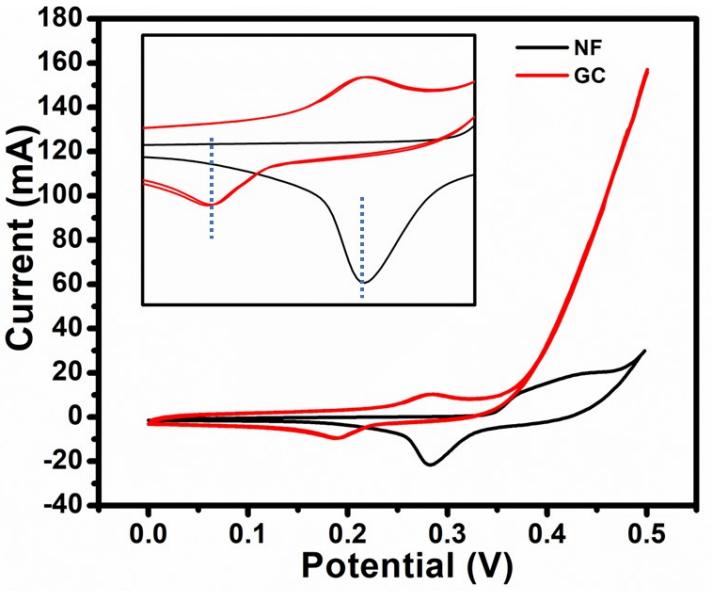

Fig. S11. Shows the cyclic voltammetry curve of NiFc-MOF on nickel foam FcDCA on a glassy carbon electrode(inset having zoomed view).

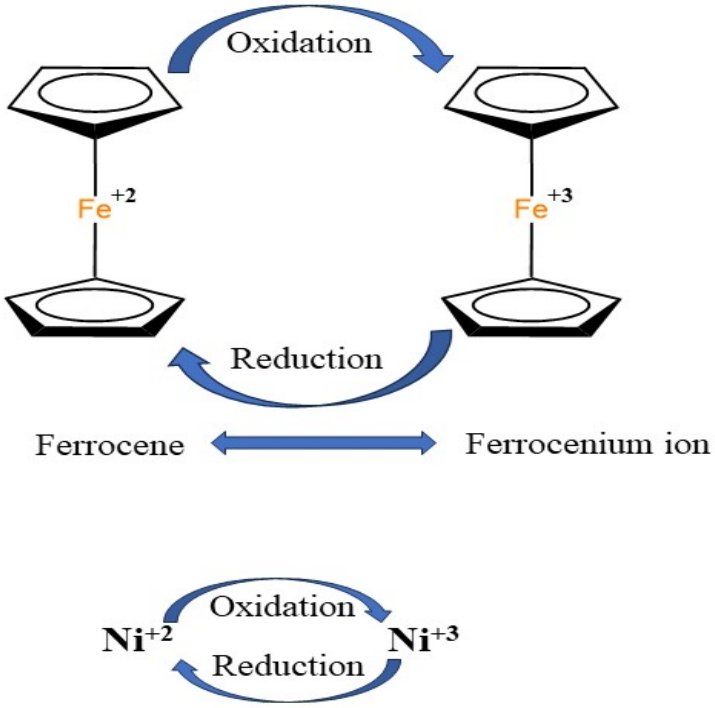

Fig. S12. The reversible oxidation-reduction process occurs in the ferrocene unit and Nickel MOF.

In the reversible oxidation-reduction process, one electron is oxidised of the ferrocene unit during the redox process, and the formed ferrocenium ion is reversed during the reduction process. Ferrocene dicarboxylic acid's oxidation peak is not clearly visible on the NF electrode. Due to overlapping redox signals from NF and Ni-MOF, the oxidation and reduction peaks of ferrocene dicarboxylic acid were absent. When NF is used as the working electrode, a sizable background current is seen based on the following literature.[2,3] Furthermore, the Nickel undergoes one electron oxidation-reduction process. The above mechanism is concluded based on the following literature[2,3].

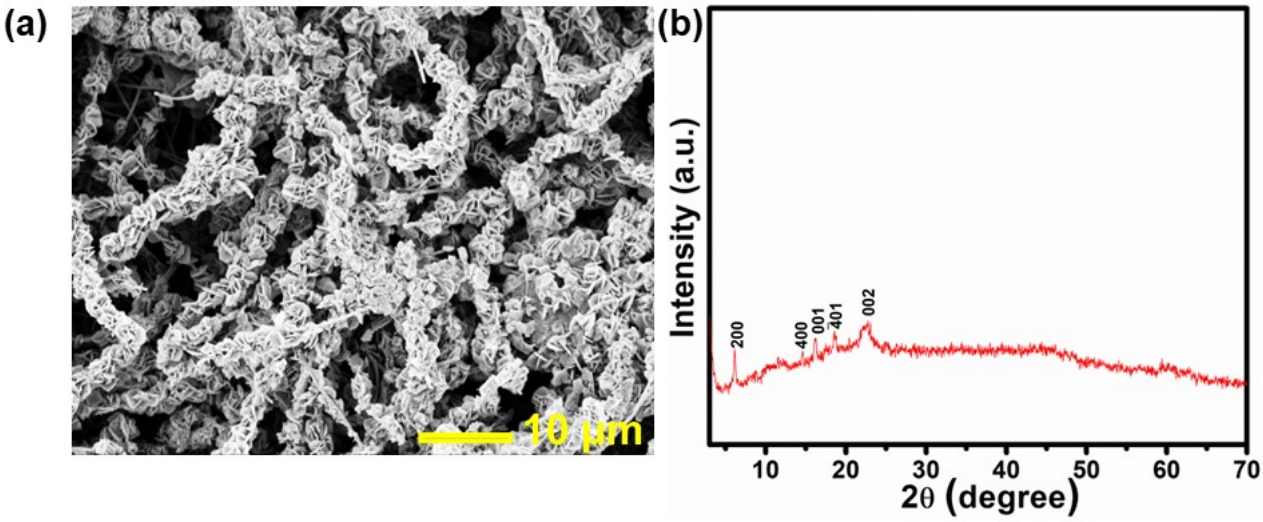

Fig. S13. (a) SEM (b) PXRD analysis of NiFc-MOF@CNF after electrochemical performance.

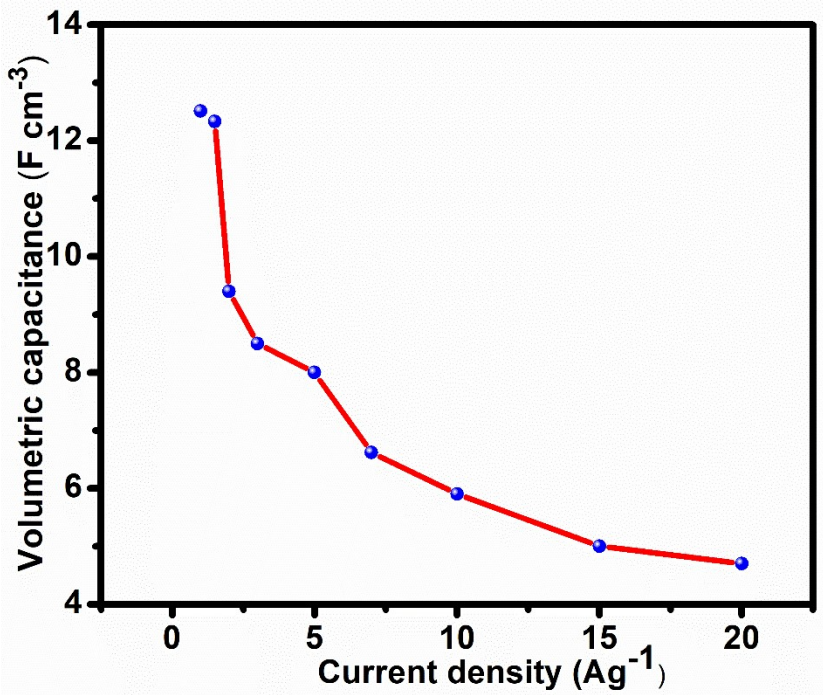

Fig. S14. Shows the volumetric capacitance at different current densities.

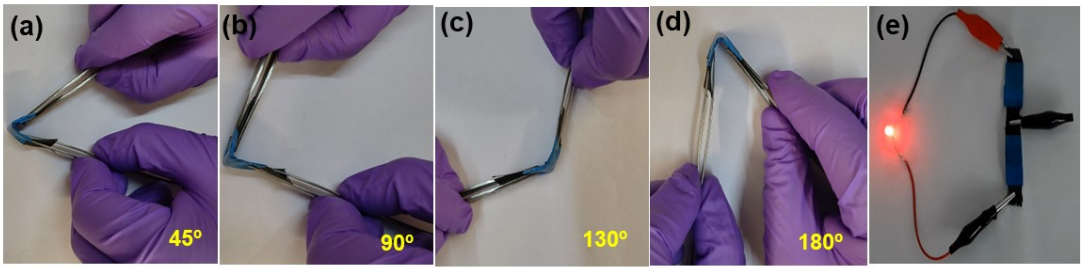

Fig. S15 (a-d) Photograph of the flexible device at different angles (e) Enlightened LED bulb.

Table S1. Percentage compositions of NiFc-MOF@CNF.

Sr. No	Elements	(%) compositions
1	Ni	7.62
2	Fe	7.99
3	C	52.26
4	O	30.77
5	N	1.37

Table. S2 Comparison of electrochemical performance of redox-active Nifc-MOF@CNF with the previous MOF/ MOF nanofiber-based electrode.

S. No.	Electrode materials	Specific capacitance/ Capacity (Fg^{-1})/ (Cg^{-1})	Current density (Ag^{-1})	Cycling stability	Ref.
1	MOF/MXene nanofiber derived MX-5@PCNF	572Fg^{-1}	1Ag^{-1}	71.24% after 10,000 Cycles	**J. Mater. Chem. A,** 2023, 11, 5001–5014
2	MOF@CNF derived Co–S@CNF–CNT-3	416.6 Fg^{-1}	0.2 Ag^{-1}	96.6% after 10,000 Cycles	**J. Mater. Chem. C,** 2022, 10, 542–548
3	CNF@Ni-CAT MOF	502.95 Fg^{-1}	0.5 Ag^{-1}	73% after 10,000 Cycles	**Inorg. Chem. Front.,** 2019, 6, 1824–1830
4.	c-MOF@CNF	125 Fg^{-1}	0.33 Ag^{-1}	90% after 10,000 cycles	**ACS Nano** 2019, 13, 9578−9586
5	Co-MOF@MXene nanofiber derived Co-PC@MX-CNF	426.7 Fg^{-1}	1 Ag^{-1}	90.36% after 10,000 Cycles	**Chem. Eng. J** 2022, 437, 135338
6	FOCNF NOCNF	523 Fg^{-1} 468 Fg^{-1}	1 Ag^{-1} 1 Ag^{-1}	81.3% after 10,000 Cycles	**Small Struct.** 2022, 3, 2200015
7	PAN/ZIF-based HPCNFs	307.2 Fg^{-1}	1 Ag^{-1}	98.2% after 10,000 Cycles	***Energy Environ. Sci.***, 2017,**10**, 1777-1783
8	MOF-derived N, S co-doped CNF.	272 Fg^{-1}	0.1 Ag^{-1}	88% after 2000 Cycles	**Energy Stor. Mater**.2018, 13,72-89
9	ZIF-8/pp-SiO_2 Derived NHCSFs	253.6 Fg^{-1}	1 Ag^{-1}	92.2% after 20000 Cycles	**Carbon.** 2018, 136,176-186
10	PPNF@Co-Ni-MOF	1096.2 Fg^{-1}	1Ag^{-1}	14.5 % loss after 10,000 cycles	***ACS Appl. Mater. Interfaces*** 2020, 12, 1, 1280–1291
11	**Redox active NiFc-MOF@CNF**	**460 Cg^{-1} (1150 F^{-1})**	**1Ag^{-1}**	**82.2% after 25,000 Cycles**	**This Work**

References

1 I. Pathak, D. Acharya, K. Chhetri, P. C. Lohani, S. Subedi, A. Muthurasu, T. Kim, T. H. Ko, B. Dahal and H. Y. Kim, *J. Mater. Chem. A*, 2023, **11**, 5001–5014.

2 J. Benecke, S. Mangelsen, T. A. Engesser, T. Weyrich, J. Junge, N. Stock and H. Reinsch, *Dalton Trans.*, 2019, **48**, 16737–16743.

3 J. Liang, X. Gao, B. Guo, Y. Ding, J. Yan, Z. Guo, E. C. M. Tse and J. Liu, *Angewandte Chemie International Edition*, 2021, **60**, 12770–12774.